Optical response and activity of ultrathin films of topological insulators

Fariborz Parhizgar,[1,*] Ali G. Moghaddam,[1,2,†] and Reza Asgari[1,‡]
[1]*School of Physics, Institute for Research in Fundamental Sciences (IPM), Tehran 19395-5531, Iran*
[2]*Department of Physics, Institute for Advanced Studies in Basic Science (IASBS), Zanjan 45137-66731 Iran*
(Received 11 December 2014; published 27 July 2015)

We investigate the optical properties of ultrathin film of a topological insulator in the presence of an in-plane magnetic field. We show that due to the combination of the overlap between the surface states of the two layers and the magnetic field, the optical conductivity can show strong anisotropy. This leads to the effective optical activity of the ultrathin film by influencing the circularly polarized incident light. Intriguingly, for a range of magnetic fields, the reflected and transmitted lights exhibit elliptic character. Even for certain values almost linear polarizations are obtained, indicating that the thin film can act as a polaroid in reflection. All these features are discussed in the context of the time-reversal symmetry breaking as one of the key ingredients for the optical activity.

DOI: 10.1103/PhysRevB.92.045429 PACS number(s): 78.20.Ls, 78.67.−n, 75.85.+t

I. INTRODUCTION

Optical activity of a material which refers to its effect on the polarization of light passing through it in general originates from some symmetry breaking or anisotropy in the structure of materials [1,2]. Magneto-optical effects, which are known for more than one and a half century, have in particular their roots in the time-reversal symmetry (TRS) breaking in the presence of a magnetic field. Besides, magneto-optical effects have applications in measuring instruments, optical devices, and chemical characterizations [3,4]. Recently, investigations about the optical properties of low-dimensional and especially two dimensional (2D) systems have increased a lot motivated by synthesis of a variety of 2D materials including graphene [5], monolayers of transition metal dichalcogenides [6], and also the thin film of the topological insulators (TIs) [7,8]. A great advantage of all these 2D systems is the tunability of their electronic structure by electric or magnetic fields which leads to many promising applications in nanoelectronics, spintronics, as well as optical and photonic devices.

Among all of the above-mentioned new materials, the discovery of the TI is of more fundamental importance since it opens new lines of investigation in the theory of condensed-matter physics [9,10]. In particular, by reformulating the band theory, providing better understanding of topological orders, and contributing to the field of the quantum information and quantum computing, topological insulators are in the heart of interest in recent years [7,8]. Topological insulators in three dimensions are insulating materials in which the strong spin-orbit interaction causes the band inversion [11]. At the surface of the TI, the bands turn back to their natural order and subsequently topologically protected surface states emerge. These states usually governed by some relativistic dynamics persist a robust gapless dispersion unless the TRS is broken by applying magnetic fields or in the presence of magnetic impurities.

The strong sensitivity of the TI to any perturbation which breaks the TRS leads to interesting phenomena in their magneto-optical responses [12–14]. A key finding has been provided by Tse and MacDonald revealing a giant magneto-optical Kerr effect besides a universal Faraday angle, $\theta_F = \arctan(\alpha)$ where the fine-structure constant is $\alpha = e^2/\hbar c$, at the long-wavelength limit [15–17]. They considered a thin film of the TI in the presence of a perpendicular magnetic field which can be described by the microscopic 2D massless Dirac model. Then using the linear-response theory rather than topological field theory method [10], the optical conductivity and the magneto-optical responses have been obtained. As a result of the interplay between confinement and the Hall effect of Dirac modes, only quantized currents are induced by the incident electromagnetic waves and subsequently the reflected and transmitted waves show an unexpected behavior. However, the TRS breaking and the gap opening due to the magnetic field play an important role in the observation of these optical phenomena.

Remarkably, the optical conductivity of the TI surface states and a thin film of the TI have been studied theoretically [18–20] and the universal value for the optical conductivity, $\sigma_0 = e^2/4\hbar$, has been obtained. Moreover, the optical properties of bismuth-based topological insulators have been experimentally explored [21]. Intriguingly enough, it has been predicted [22–24] and verified experimentally that the surface states of the two sides of thin film hybridize with each other when the thickness of TI thin films becomes less than six quintuple layers (QLs) [25]. Subsequently, the hybridization via quantum tunneling opens a gap Δ in the band structure, which varies in an oscillatory manner with the thin-film thickness [22–24]. The variation of thin-film thickness can even lead to the change of the surface band Chern numbers and their topological properties [24].

In this paper, we analyze the optical responses of ultrathin films of the TI in the presence of the in-plane magnetic field B and the gap due to the overlap between the surface states. One should note that this gap appears without TRS breaking unlike the case that an out-of-plane magnetic field or magnetic impurities are present. The effect of the in-plane magnetic field is a constant difference in the vector potential

*fariborz.parhizgar@ipm.ir
†agorbanz@iasbs.ac.ir
‡asgari@ipm.ir

of the surface states at the two sides. Without hybridization of surface states such difference can be gauged out without any physical effect, however the overlap between them prohibits independent gauge transformations for two sides. Therefore, the combination of the in-plane magnetic field and hybridization leads to the interesting behavior of their optical responses.

We show that the optical conductivity tensor exhibits a profound anisotropy and its longitudinal components σ_{xx} and σ_{yy} change drastically by the variation of the imposed field. Competition between the hybridization and an energy scale proportional to B leads to two different phases of the system. In small B values, the thin film exposes a gapped dispersion relation, however at some certain value of the magnetic field, the gap closes and the system enters into a gapless phase. Some qualitative differences in the behavior of the optical conductivity are found in those two phases. Then we investigate the properties of the reflected and transmitted electromagnetic waves when a right-handed circularly polarized light is incident normally on the system. Intriguingly, we obtain, for some certain range of the B around the band structure, phase transition, the reflected light becomes elliptic and even nearly linearly polarized while the transmitted one always remains close to the circular polarization. Far away from the transition, i.e., for very small B or Δ, the time-reversal symmetry is restored and the system behaves similar to a simple isotropic metal.

This paper is organized as follows. Sec. II is devoted to the theoretical model and basic formalisms. First, a model Hamiltonian of the system is introduced and then the conductivities are calculated by using Kubo formalism. The model for the optics and propagation of the electromagnetic waves through thin film is given. In Sec. III we present our numerical results. Finally, we conclude our main results in Sec. IV.

II. MODEL AND THEORY

Our model consists of a thin film of TI with the width d in the direction normal to the plane of the system (z) at zero temperature and having translational symmetry in the x-y plane. As shown in several works, one can use the low-energy Hamiltonian proposed for the bulk TI in the vicinity of the Γ point to describe the low-energy behavior of the ultrathin film versus the in-plane momentum $\mathbf{k} = (k_x, k_y)$. Taking into account the four hybridized p_z orbitals denoted by $|\tau, s\rangle = |p_z^{\tau}, s\rangle$ where $\tau = \pm 1$ show even and odd parities and $s = \uparrow, \downarrow$ is the spin, the Hamiltonian of the thin film takes the following form [24]:

$$\mathcal{H}_{3D} = C - D_1\partial_z^2 + D_2k^2 + \begin{pmatrix} \mathcal{M}(\mathbf{k})\sigma_z - iA_1\sigma_x\partial_z & A_2k_-\sigma_x \\ A_2k_+\sigma_x & \mathcal{M}(\mathbf{k})\sigma_z + iA_1\sigma_x\partial_z \end{pmatrix}. \quad (1)$$

Here $k_\pm = k_x \pm k_y$, $k = \sqrt{k_x^2 + k_y^2}$ are moments, $\mathcal{M}(k) = M + B_1\partial_z^2 - B_2k^2$ is the momentum dependent mass term and constants A_1, A_2, B_1, B_2, C, D_1, D_2, and M are the model parameters which can be fitted from experiment or *ab initio* calculations.

In order to find the effective 2D Hamiltonian for the ultrathin film of a TI, one can first find the general surface-state solutions of the above three-dimensional (3D) Hamiltonian (1) imposing the boundary conditions at $z = \pm d/2$. Then by projecting the 3D Hamiltonian into the space of surface states we end up with the effective 2D Hamiltonian H_{2D}. It is known that the ultrathin film of a TI in the absence of magnetic field can be described using two degenerate massive Dirac hyperbolas which are each other's time-reversal counterpart. The effective Hamiltonian leading to such Dirac dispersions can be obtained choosing a variety of bases. One way is to work in the direct product space of the real spin $\boldsymbol{\sigma}$ and the subspace of two hyperbolas denoted by $\tau_z = \pm 1$ as carried out by several groups [22–27]. This approach after some algebra yields the following Hamiltonian:

$$\mathcal{H}_{2D} = \tau_0 \otimes [(E_0 - Dk^2)\sigma_0 - h(\mathbf{k})] + \tau_z \otimes \sigma_z\Delta(\mathbf{k}), \quad (2)$$

in which $h(\mathbf{k}) = \hbar v\hat{z}(\hat{\sigma} \times \mathbf{k})$ is the Dirac Hamiltonian and $\Delta(\mathbf{k}) = \Delta_0 - Bk^2$. Here $\hat{z}$ shows the direction perpendicular to the upper surface, $\hat{\sigma}$ indicates the Pauli matrices for the real spin. The parameters E_0, Δ_0, D, B in general depend on the geometry of the thin film (d) and should be obtained self-consistently by fitting the Hamiltonian to the experimental band structure. Assuming the width $W = 5$ QLs we use the numerical values given in Ref. [25] as $\Delta_0 = 0.041$ meV, $D = -15.3$ eV Å^{-2}, $B = 5$ eV Å^{-2}, and $v = 4.53 \times 10^5$ m/s is the Fermi velocity of the helical states in the TI.

An alternative approach to the effective 2D Hamiltonian is to work in the subspaces of the spin and two side surface states assuming a general $\mathbf{k}$-dependent hybridization $\Delta(\mathbf{k})$ coupling the two surfaces [28]. This particular description is useful when we have in-plane magnetic field and its effect on the different surface states can be simply introduced in a gauge invariant form. The basis in this regard has four kets $|u\uparrow\rangle$, $|u\downarrow\rangle$, $|d\uparrow\rangle$, $|d\downarrow\rangle$ in which $u(d)$ denotes the top (bottom) surface. Using a unitary transformation we can obtain a new effective Hamiltonian from Eq. (2) as

$$\mathcal{H}_{\text{eff}}(\mathbf{k}) = E_0 - Dk^2 + \begin{pmatrix} h(\mathbf{k}) & \Delta(\mathbf{k}) \\ \Delta(\mathbf{k}) & -h(\mathbf{k}) \end{pmatrix}. \quad (3)$$

Applying a magnetic field parallel to the single surface of the TI just shifts the position of the Dirac cone in the momentum space and can be gauged out without any physical implications. While in the case of ultrathin films, as mentioned above, the in-plane magnetic field induces two different gauge shifts in two different surfaces and subsequently the band dispersion can be affected by B. For the sake of definiteness, we consider $\mathbf{B} = B_y\hat{y}$ which leads to the gauge field $A = zB_y\hat{x}$ and as a result [29] one can write the new Hamiltonian as

$$\mathcal{H}_{\text{eff}}(\mathbf{k}, \mathbf{q}_B) = E_0 - \begin{pmatrix} D|\mathbf{k} - \mathbf{q}_B|^2 & 0 \\ 0 & D|\mathbf{k} + \mathbf{q}_B|^2 \end{pmatrix} + \begin{pmatrix} h(\mathbf{k} - \mathbf{q}_B) & \Delta(\mathbf{k}) \\ \Delta(\mathbf{k}) & -h(\mathbf{k} + \mathbf{q}_B) \end{pmatrix}, \quad (4)$$

where $\mathbf{q}_B = eB_yd/2\hbar\hat{\mathbf{x}}$. Due to the geometry under consideration and the gauge invariance, the hybridization terms are not affected by the in-plane magnetic field.

In the absence of the in-plane magnetic field, the electronic band structure is isotropic in terms of the momentum $\mathbf{k}$ and

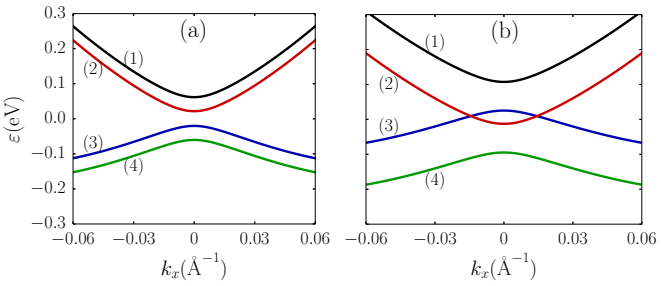

FIG. 1. (Color online) Dispersion of the topological insulator thin film along in the k_x direction at the presence of an in-plane magnetic field and a hybridization Δ_0. Left and right panels correspond to (a) $\varepsilon_B = 0.02$ eV ($\varepsilon_B < \Delta_0$) and (b) $\varepsilon_B = 0.06$ eV ($\varepsilon_B > \Delta_0$), respectively.

consists of two double degenerate bands separated by the gap Δ_0 at $k = 0$. The presence of the magnetic field results in the anisotropy of the bands dispersion. Considering the dispersion relation along the x direction $\varepsilon(k_x)$, two different phases can be distinguished depending on the value of the magnetic momentum q_B, as discussed in Ref. [30] for the simpler effective model containing only linear terms in momentum. The predicted quantum phase transition is due to the competition between the gap Δ_0 and the magnetic cyclotron energy $\varepsilon_B = \hbar v q_B$ as illustrated in Fig. 1. In small magnetic fields where $\varepsilon_B < \Delta_0$, the system is gapped while at $\varepsilon_B > \Delta_0$, two subbands intersect subsequently at the zero energy and close the gap. It is worth noting that for a thin film with thickness 5 QLs (∼7 nm) a magnetic field of the order $B \approx 23$ T is needed to reach a typical cyclotron energy of $\varepsilon_B = 0.041$ eV. Such a magnetic field is indeed quite large but at the same time accessible in experiments.

A. Optical conductivity of the thin-film TI

In order to calculate the optical conductivity tensor $\sigma_{\alpha\beta}(\omega)$, we invoke the linear-response theory and the Kubo formula given by [16,31]

$$\sigma_{\alpha\beta}(\omega) = i \sum_k \sum_{\mu\mu'} \frac{f_{k,\mu} - f_{k,\mu'}}{\varepsilon_{k,\mu} - \varepsilon_{k,\mu'}} \frac{\mathcal{J}^{\mu\mu'}_{\alpha\beta}(k)}{\hbar\omega + \varepsilon_{k\mu} - \varepsilon_{k\mu'} + i/2\tau_s}, \tag{5}$$

where μ,μ' denote the different bands and α,β indicate x,y axes. The Fermi-Dirac distribution function is indicated by $f_{k,\mu}$ at the Fermi level μ and $\tau_s = 1/\Gamma$ is a tiny residual scattering time due to impurities. The tensor quantity $\mathcal{J}^{\mu\mu'}_{\alpha\beta}(k) = \langle k,\mu|j_\alpha|k,\mu'\rangle\langle k,\mu'|j_\beta|k,\mu\rangle$ is given by the components of the current operator $j_\alpha = e\partial H/\partial k_\alpha$ which for the ultrathin film of the TI reads as

$$j_\alpha = -e\begin{pmatrix} 2Dk_\alpha - q_B\delta_{x\alpha} & 0 \\ 0 & 2Dk_\alpha + q_B\delta_{x\alpha} \end{pmatrix} + e\begin{pmatrix} \mp\hbar v\sigma_{\bar\alpha} & -2Bk_\alpha \\ -2Bk_\alpha & \pm\hbar v\sigma_{\bar\alpha} \end{pmatrix}, \tag{6}$$

where $\delta_{x\alpha}$ is the Kronecker δ and α ($\bar\alpha$) denotes x or y (y or x). In our model, since there is no longer perpendicular magnetic field or magnetization, the Hall conductivity vanishes, $\sigma_{xy} = 0$ however, the in-plane field makes the conductivity strongly anisotropic, namely $\sigma_{xx} \neq \sigma_{yy}$. We include only the interband transitions at zero-Fermi energy and the contribution of the intraband transitions, which leads to a Drude-like term, is no longer relevant in this study since the momentum relaxation time is assumed to be very large. This approximation is valid at low temperature and a quite clean sample. We also do not consider the bound state of exciton in the system. To be precise, the phenomenological scattering rate Γ is chosen to be $\Gamma = 1$ meV which originates from possible impurity and defects in the system [16]. Remarkably, we note that in the undoped case, $E_F = 0$, the Kubo formula only includes the interband conductivity and thus the intraband part ($\mu = \mu'$) vanishes.

In order to calculate the optical conductivities we need to find the dispersion relations of different bands $\varepsilon_{k,\mu}$ as well as the eigenstates $|k,\mu\rangle$. For the effective Hamiltonian (4) which contains up to quadratic terms in momentum, the energy and eigenstates can be calculated numerically and we do not present the lengthy analytical expressions. Throughout the paper we will use the full quadratic model and the presented results for the optical conductivities and other quantities determining the optical activities are calculated numerically based on this model. However in order to enrich our discussion in what follows, we will present the analytical expressions which are available for the simplified Hamiltonian containing up to linear terms in momentum.

B. Simplified low-energy model

In this part, we discuss the simple model in which only the terms up to linear in $\mathbf{k}$ are kept, and then present analytical expressions of the eigenstates and the tensors $\mathcal{J}_{\alpha\beta}$. We should remind that this simple picture is verified if we concentrate on very low-energy properties of the thin film, as employed in many other works [28,30,32–37]. The simplified Hamiltonian of an ultrathin film of TI at the presence of the in-plane magnetic field can be written as

$$\mathcal{H}_{\rm sim} = \begin{pmatrix} h(\mathbf{k} - \mathbf{q}_B) & \Delta_0 \\ \Delta_0 & -h(\mathbf{k} + \mathbf{q}_B) \end{pmatrix}. \tag{7}$$

The energy dispersion for this model has the form $\varepsilon_{s,t,\mathbf{k}} = s\sqrt{\hbar^2v^2k^2\sin^2\phi + g_t^2(k)}$ with $g_t(k) = \hbar v q_B + t\sqrt{\hbar^2v^2k^2\cos^2\phi + \Delta_0^2}$. Here $s = \pm1$ shows the valance ($s = -1$) and conduction ($s = +1$) bands and $t = \pm1$ indicates the bands with larger and smaller gaps, respectively. From the above expression it is clear that the presence of the magnetic field leads to the anisotropy of the dispersion relation indicated by the explicit dependence on the momentum direction angle $\phi = \arctan(k_y/k_x)$.

After straightforward algebra, the four eigenfunctions of the Hamiltonian Eq. (7) indicated by $|s,t\rangle$ are obtained as

$$|s,+\rangle = \frac{1}{\sqrt{2}}\begin{pmatrix} i\sin\frac{\gamma}{2}e^{i\theta_+} \\ -s\sin\frac{\gamma}{2} \\ is\cos\frac{\gamma}{2} \\ -\cos\frac{\gamma}{2}e^{i\theta_+} \end{pmatrix}, \quad |s,-\rangle = \frac{1}{\sqrt{2}}\begin{pmatrix} i\cos\frac{\gamma}{2}e^{i\theta_-} \\ -s\cos\frac{\gamma}{2} \\ -is\sin\frac{\gamma}{2} \\ \sin\frac{\gamma}{2}e^{i\theta_-} \end{pmatrix}, \tag{8}$$

with the newly defined parameters γ and θ_t in order that $\sin\gamma = \Delta_0/\sqrt{\hbar^2v^2k^2\cos^2\phi + \Delta_0^2}$, $\sin\theta_t = \hbar vk\sin\phi/\sqrt{\hbar^2v^2k^2\sin^2\phi + g_t^2(k)}$.

Using the wave functions from Eq. (8) and the basis as $\psi^\dagger_{s,t} = (\psi^\dagger_{+,+},\psi^\dagger_{+,-},\psi^\dagger_{-,-},\psi^\dagger_{-,+})$, the longitudinal parts of the quantity $\mathcal{J}^{\mu\mu'}_{\alpha\alpha}(k)$ are given by

$$\mathcal{J}_{xx}(k) = \begin{pmatrix} \cos^2\gamma\cos^2\theta_+ & \sin^2\gamma\cos^2\frac{\theta_+ + \theta_-}{2} & \sin^2\gamma\sin^2\frac{\theta_+ + \theta_-}{2} & \cos^2\gamma\sin^2\theta_+ \\ \sin^2\gamma\cos^2\frac{\theta_+ + \theta_-}{2} & \cos^2\gamma\cos^2\theta_- & \cos^2\gamma\sin^2\theta_- & \sin^2\gamma\sin^2\frac{\theta_+ + \theta_-}{2} \\ \sin^2\gamma\sin^2\frac{\theta_+ + \theta_-}{2} & \cos^2\gamma\sin^2\theta_- & \cos^2\gamma\cos^2\theta_- & \sin^2\gamma\cos^2\frac{\theta_+ + \theta_-}{2} \\ \cos^2\gamma\sin^2\theta_+ & \sin^2\gamma\sin^2\frac{\theta_+ + \theta_-}{2} & \sin^2\gamma\cos^2\frac{\theta_+ + \theta_-}{2} & \cos^2\gamma\cos^2\theta_+ \end{pmatrix} \tag{9}$$

and

$$\mathcal{J}_{yy}(k) = \begin{pmatrix} \sin^2\theta_+ & 0 & 0 & \cos^2\theta_+ \\ 0 & \sin^2\theta_- & \cos^2\theta_- & 0 \\ 0 & \cos^2\theta_- & \sin^2\theta_- & 0 \\ \cos^2\theta_+ & 0 & 0 & \sin^2\theta_+ \end{pmatrix}. \tag{10}$$

Furthermore, for the Hall conductivity part, we can write the $\mathcal{J}_{yx}(k)$ as

$$\mathcal{J}_{yx}(k) = \frac{\cos(\gamma)}{2} \times \begin{pmatrix} \sin 2\theta_+ & 0 & 0 & \sin 2\theta_+ \\ 0 & -\sin 2\theta_- & -\sin 2\theta_- & 0 \\ 0 & -\sin 2\theta_- & -\sin 2\theta_- & 0 \\ \sin 2\theta_+ & 0 & 0 & \sin 2\theta_+ \end{pmatrix}; \tag{11}$$

since all the terms of $\mathcal{J}_{yx}(k)$ are odd in θ, we thus conclude that $\sigma_{yx} = 0$ as discussed before.

Based on Eqs. (9) and (10), we are able to explore the selection rules of the optical conductivity in the system. For the sake of clarification, let us label the eigenfunctions by $(s,t) = (+,+),(+,-),(-,-),(-,+)$ and corresponding bands shown in Fig. 1 with numbers from 1 to 4, respectively. As seen in Eq. (10), the transitions $3 \to 1$ and $4 \to 2$ are forbidden. Also later on, we show numerically that although all transitions are allowed for σ_{xx}, the transitions $3 \to 2$ and $4 \to 1$ are negligible and have a minor effect. Note that in this paper, we assume $E_F = 0$ so the transitions $3 \to 4$ and $1 \to 2$ are unimportant regardless of the $\mathcal{J}$ values.

C. Propagation of electromagnetic waves through the thin film TI

Here, we explore the properties of the reflected and transmitted electromagnetic waves of an incident wave which are completely given by the optical conductivity tensor. We assume that the thin film lies in the x-y plane and the incident and scattered lights which are plane waves propagate in the z direction normal to the thin-film plane. The intensity, phase, and polarization of the electromagnetic waves can be obtained from their electric fields $\mathbf{E}^i$, $\mathbf{E}^r$, and $\mathbf{E}^t$ at $z = 0$ corresponding to the incident, reflected, and transmitted parts. We should remind that the electric field here is a complex two-component vector $\mathbf{E} = E_x\hat{\mathbf{x}} + E_y\hat{\mathbf{y}}$. The reflected and transmitted waves are related to the incident one with linear relations $\mathbf{E}^r = \hat{\mathbf{r}}\mathbf{E}^i$ and $\mathbf{E}^t = \hat{\mathbf{t}}\mathbf{E}^i$ in which $\hat{\mathbf{r}}$ and $\hat{\mathbf{t}}$ are 2×2 complex matrices in the two-dimensional space corresponding to the x-y plane. If we ignore the thickness of the thin film in comparison with the wavelength and denote the field in the two sides of the film with $\mathbf{E}^{(u)}$ and $\mathbf{E}^{(d)}$, then the boundary conditions for the electric and magnetic fields will be $\mathbf{E}^{(u)} = \mathbf{E}^{(d)}$ and $-i\hat{t}_y(\mathbf{H}^{(u)} - \mathbf{H}^{(d)}) = (4\pi/c)\mathbf{J} = (4\pi/c)\hat{\boldsymbol{\sigma}}\mathbf{E}$. Assuming the incident light hits the upper side of the film, the electric fields of the two sides are given by $\mathbf{E}^{(u)} = \mathbf{E}^i + \mathbf{E}^r$ and $\mathbf{E}^{(d)} = \mathbf{E}^t$ and magnetic fields follows the corresponding relations. Adding to these relations and the boundary conditions, the fact that for the vacuum at each side $\mathbf{H} = \hat{\mathbf{z}} \times \mathbf{E}$, we derive the transmission and reflection matrices as

$$\hat{\mathbf{r}} = \begin{pmatrix} \frac{-\tilde{\sigma}_{xx}}{\tilde{\sigma}_{xx}+2} & 0 \\ 0 & \frac{-\tilde{\sigma}_{yy}}{\tilde{\sigma}_{yy}+2} \end{pmatrix}, \quad \hat{\mathbf{t}} = \begin{pmatrix} \frac{2}{\tilde{\sigma}_{xx}+2} & 0 \\ 0 & \frac{2}{\tilde{\sigma}_{yy}+2} \end{pmatrix}, \tag{12}$$

where $\tilde{\sigma}_{\alpha\beta} = (4\pi/c)\sigma_{\alpha\beta}$ denotes the dimensionless conductivity.

Now, we suppose a right-circularly polarized electromagnetic wave of the form $\mathbf{E}^i = E_0(\hat{\mathbf{x}} + i\hat{\mathbf{y}})/\sqrt{2}$ is incoming to the TI plane. Due to the anisotropic conductivity ($\sigma_{xx} \neq \sigma_{yy}$), which is a consequence of the in-plane magnetic field, the reflected and transmitted waves will be of elliptical polarization as

$$\begin{aligned} \mathbf{E}^{\mathbf{r}} &= E_0(r_{xx}\hat{\mathbf{x}} + ir_{yy}\hat{\mathbf{y}})/\sqrt{2}, \\ \mathbf{E}^t &= E_0(t_{xx}\hat{\mathbf{x}} + it_{yy}\hat{\mathbf{y}})/\sqrt{2} \end{aligned} \tag{13}$$

in which the components of matrices $\hat{\mathbf{r}}$ and $\hat{\mathbf{t}}$ are defined in Eq. (12). It is more convenient to use the circular polarization bases given by $\hat{\boldsymbol{\epsilon}}_\pm = (\hat{\mathbf{x}} \pm i\hat{\mathbf{y}})/2$ indicating the right- and left-handed circular polarizations, respectively [38]. The general elliptically polarized wave is thus described with $\mathbf{E} = E_+\hat{\boldsymbol{\epsilon}}_+ + E_-\hat{\boldsymbol{\epsilon}}_-$.

The eccentricity and the rotation angle of the polarization ellipse are given by $e_P = 2/(\sqrt{|E_+/E_-|} + \sqrt{|E_-/E_+|})$ and $\alpha_P = (\varphi_+ - \varphi_-)/2$ in which $\varphi_\pm = \arg E_\pm = \arctan(\mathrm{Im}E_\pm/\mathrm{Re}E_\pm)$. Then by invoking Eq. (13), the eccentricity and rotation angle of the reflected electromagnetic wave are

$$e^r_P = \frac{2}{\sqrt{\left|\frac{r_{xx}-r_{yy}}{r_{xx}+r_{yy}}\right|} + \sqrt{\left|\frac{r_{xx}+r_{yy}}{r_{xx}-r_{yy}}\right|}}, \tag{14}$$

$$\alpha^r_P = \frac{1}{2}\arg\left(\frac{r_{xx}+r_{yy}}{r_{xx}-r_{yy}}\right), \tag{15}$$

and the transmitted part obeys the corresponding relation with $r_{\alpha\alpha}$ replaced by $t_{\alpha\alpha}$. It is clear that the anisotropy in the optical conductivity leads to the difference in the reflection and transmission components ($r_{\alpha\alpha}$ and $t_{\alpha\alpha}$). In general, we have elliptically polarized scattered waves with a nonvanishing eccentricity. We should remind that the eccentricity is a measure of ellipticity, varying from 0 for circular polarizations to 1 corresponding to the linearly polarized waves.

Using the matrices $\hat{\mathbf{r}}$ and $\hat{\mathbf{t}}$, we obtain the intensities of reflected and transmitted waves as

$$\frac{I_r}{E_0^2} = \frac{1}{2}\sum_{\alpha}\frac{|\tilde{\sigma}_{\alpha\alpha}|^2}{(2+\mathrm{Re}\tilde{\sigma}_{\alpha\alpha})^2+(\mathrm{Im}\tilde{\sigma}_{\alpha\alpha})^2},$$
$$\frac{I_t}{E_0^2} = \frac{1}{2}\sum_{\alpha}\frac{4}{(2+\mathrm{Re}\tilde{\sigma}_{\alpha\alpha})^2+(\mathrm{Im}\tilde{\sigma}_{\alpha\alpha})^2}. \quad (16)$$

As a result, the absorbed wave intensity is given by

$$\frac{I_{\mathrm{abs}}}{E_0^2} = \sum_{\alpha}\frac{2\mathrm{Re}\tilde{\sigma}_{\alpha\alpha}}{(2+\mathrm{Re}\tilde{\sigma}_{\alpha\alpha})^2+(\mathrm{Im}\tilde{\sigma}_{\alpha\alpha})^2}, \quad (17)$$

which is always positive due to the fact that $\mathrm{Re}\sigma_{\alpha\alpha} > 0$. This itself originates from the second law of thermodynamics revealing power dissipation instead of the power generation.

III. NUMERICAL RESULT AND DISCUSSION

In this section, main results of our study are presented. First, the results of calculations for the optical conductivity of the ultrathin film of the TI in the presence of the in-plane magnetic field are shown as functions of the frequency ω and also the magnetic energy scale ε_B. In order to see the optical activity of the TI, we assume a circular electromagnetic wave applied perpendicularly to the sample's plane. The properties of the reflected and transmitted parts are uncovered by studying their polarizations and in particular the degree of the ellipticity and the rotation angle of the polarization ellipse. Finally, the absorption at different values of the magnetic fields is discussed. In numerical calculation we set $\Gamma = 1$ meV.

A. Optical conductivity

As we discussed in the previous section, the low-energy band structure of the system consists of four different bands which is gapped in the case that $\varepsilon_B < \Delta_0$ while the gap vanishes in the case that $\varepsilon_B \geqslant \Delta_0$. We consider the undoped system at zero temperature so that there are only four different types of transitions between those bands. The first and second types of transition occur between the bands 4 to 1 and 3 to 2, respectively, which have the largest and smallest gaps. The two other transitions are between 3 to 1 and 4 to 2 having similar energy differences. Since at zero temperature and undoped situation, the two bands 3 and 4 are filled and the others are completely empty, the two remaining transitions are forbidden.

Figure 2 shows the imaginary and real parts of the optical conductivity component σ_{xx} (scaled by $4\pi/c$) of the ultrathin film of the TI in the presence of the in-plane magnetic field in the x direction. In the gapped phase, the real part of the σ_{xx} is almost zero (apart from a small peak, according to transition from band 3 to band 2) for frequencies below $2\Delta_0$, but for higher frequencies the dissipation channel corresponding to

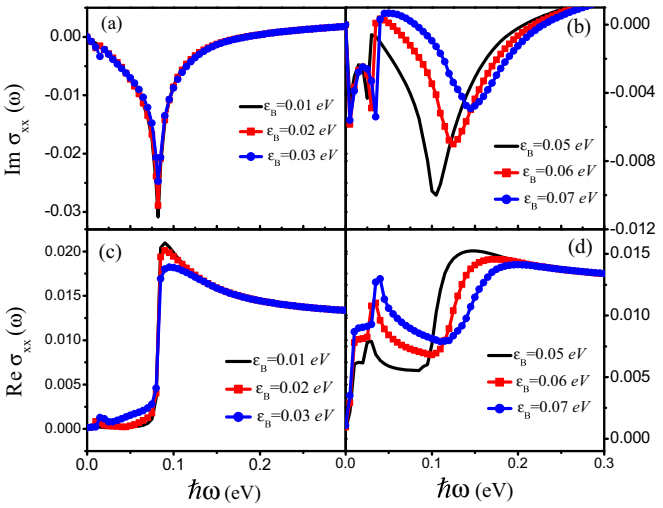

FIG. 2. (Color online) Imaginary (a),(b) and real (c),(d) parts of the optical conductivity component σ_{xx}, scaled by $4\pi/c$ as a function of the energy when $\varepsilon_B < \Delta_0$ (a),(c) and $\varepsilon_B > \Delta_0$ (b),(d). In (a),(c) the real part of the σ_{xx} is almost zero for frequencies below $2\Delta_0$, and the imaginary part shows a peak at $\omega = 2\Delta_0$ and the position of peaks and steplike configuration do not change due to the ε_B. However, the peak position does move to higher energy by increasing ε in the case (b),(d) and $\mathrm{Re}\sigma_{xx}$ shows a small peak at very low frequencies ω according to the transition between 2 and 3 band which was negligible for $\varepsilon_B < \Delta_0$.

the transitions from 3 to 1 and from 4 to 2 takes the role. On the same ground, the imaginary part shows a significant peak at $\omega = 2\Delta_0$ where the most profound photon-induced scattering of electrons between the mentioned bands is occurring. The value of the peak position for both imaginary and real parts of the longitudinal coefficient are equal as they are related by the Kramers-Kroning relations and in addition, the position of peaks and steplike configuration does not change due to the ε_B where $\varepsilon_B < \Delta_0$. However, the main peak position does move to higher energies by increasing ε_B in the case that $\varepsilon_B > \Delta_0$. Therefore, the position of peaks or steplike configuration of the dynamical conductivity can be controlled by the in-plane magnetic field. Our results in Figs. 2(a) and 2(c) indicate that although other transitions are not prohibited according to Eq. (9), they have a negligible contribution to this component of optical conductivity. When we pass through the transition point $\varepsilon_B > \Delta_0$ and the gapless phase is reached, the behavior of the conductivity changes as shown in Figs. 2(b) and 2(d). Here $\mathrm{Re}\sigma_{xx}$ shows peaks at low frequencies ω corresponding to the transition between 2 and 3 bands which were negligible for $\varepsilon_B < \Delta_0$. Another more profound jump appears due to the previously mentioned transitions from 3 to 1 and from 4 to 2 where the energy differences are not $2\Delta_0$ anymore and increases as $2\varepsilon_B$ by the variation of B. The imaginary part $\mathrm{Im}\sigma_{xx}$, subsequently, shows a strong peak at $\omega \sim 2\varepsilon_B$.

When one explores the conductivity component σ_{yy} the selection rules change and importantly, there is no transition from 3 to 1 and 4 to 2. This can be understood by using the simplified Hamiltonian and the current operator given by Eq. (10). Two other transitions at zero doping occur at two different frequencies. Figure 3 shows the behavior of σ_{yy}

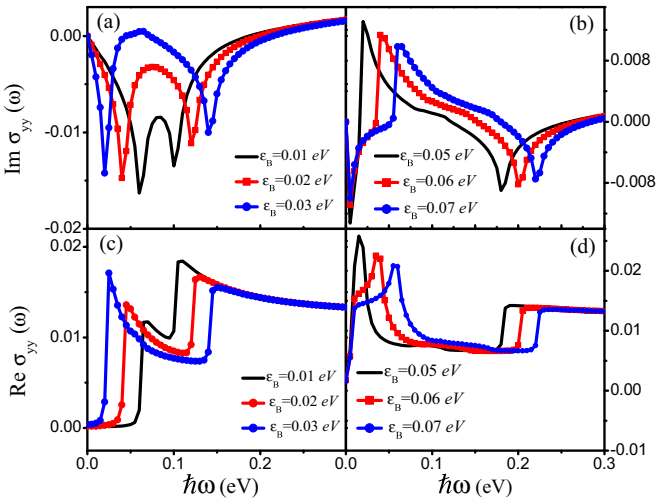

FIG. 3. (Color online) Imaginary (a),(b) and real (c),(d) parts of the optical conductivity component σ_{xx}, scaled by $4\pi/c$ as a function of the energy when $\varepsilon_B < 2\Delta_0$ (a),(c) and $\varepsilon_B > 2\Delta_0$ (b),(d). Notice that two peaks (jumps) are always present in Imσ_{xx} (Reσ_{xx}) corresponding to the smallest and largest energy differences as $2(\Delta_0 + \varepsilon_B)$ and $2|\Delta_0 - \varepsilon_B|$. The real part of the conductivity starts from a finite value and it decreases with the magnetic field.

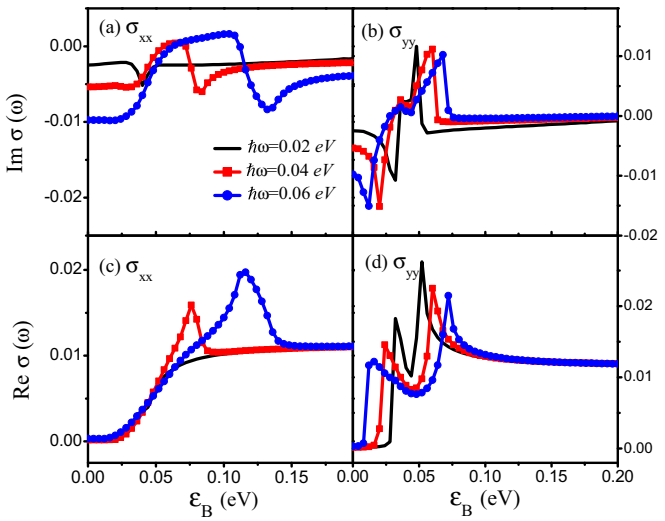

FIG. 4. (Color online) Imaginary and real parts of the optical conductivity, scaled by $4\pi/c$, of the thin-film topological insulator as a function of magnetic field energy ε_B.

(scaled by $4\pi/c$), based on the full model, at two different regimes of $\varepsilon_B < \Delta_0$ and $\varepsilon_B > \Delta_0$ as a function of ω. First for $\varepsilon_B < \Delta_0$ [panels (a) and (c)] two peaks (jumps) are always present in Imσ_{xx} (Reσ_{xx}) corresponding to the smallest and largest energy differences: $2(\Delta_0 + \varepsilon_B)$ and $2|\Delta_0 - \varepsilon_B|$. Therefore, by increasing the magnetic field the two peaks (jumps) go away from each other and at the transition point $\varepsilon_B = \Delta_0$ the first peak reaches zero frequency. On the other hand, when $\varepsilon_B > \Delta_0$ despite the gap closure, there are peaks at low frequencies corresponding to the transition between the nearest bands 2 and 3 at $k = 0$ in which they are separated. In addition, as indicated in Fig. 3(b) the behavior of the imaginary part of the conductivity is different and it can be positive in contrast to the gapped phase.

In order to conclude these results we also plot the conductivities σ_{xx} and σ_{yy} as a function of ε_B for different values of ω in Fig. 4. First of all, we see that the real part of the conductivities σ_{xx} and σ_{yy} starts from zero corresponding to the dissipationless gapped regime. Moreover, at very large magnetic fields in which $\varepsilon_B \gg \Delta_0$ and irrespective of the frequency, the conductivities tend to a constant finite value. The dissipative component Reσ_{xx} is much larger in the gapless phase ($\varepsilon_B > \Delta_0$) in comparison with the gapped one ($\varepsilon_B < \Delta_0$), a behavior which is shown in Fig. 4(c). The variation of imaginary and real parts of σ_{yy} with a magnetic field are shown in Figs. 4(b) and 4(d). Both parts reveal two peaks where one of them occurs at $\varepsilon_B < \Delta_0$ and the other at larger magnetic fields $\varepsilon_B > \Delta_0$. In addition, although the real part of σ_{yy} usually takes higher values for the gapless case $\varepsilon_B > \Delta_0$ similar to σ_{xx}, Imσ_{yy} changes sign close to the transition point showing almost antisymmetric form around $\varepsilon_B = \Delta_0$.

As a final remark at this part we note that the variations and also anisotropy in the conductivity tensor take place in the vicinity of transition points where both the magnetic field energy ε_B and the overlap Δ_0 are finite. When either ε_B or Δ_0 becomes much smaller than the other, the conductivities reach some limiting values which are the same for σ_{xx} and σ_{yy}. In particular the real parts of both components vanish at very small fields $\varepsilon_B \ll \Delta_0$ and the imaginary parts reach zero for small overlaps $\Delta_0 \ll \varepsilon_B$. These are clear signatures of the fact that for vanishing ε_B or Δ_0 in fact the time-reversal symmetry is not broken since either there is no magnetic field or it has no physical effect and can be omitted by a gauge transformation.

B. Optical activity of ultrathin films of the TI

In the following, we would like to investigate the effect of the magnetic field on the optical activity of the ultrathin films when a circularly polarized light hits the film in a normal direction. This is revealed by the phase shift α_P and eccentricity e_P of the reflected and transmitted electromagnetic waves. Figure 5 shows the behavior of the parameters e_P and α_P defined in Eqs. (14) and (15) for the reflected and transmitted components, respectively. As we apply a circularly polarized electromagnetic wave to the plane of the TI thin film, due to the anisotropy in the conductivity, the reflected and transmitted waves will not be circular anymore but they are elliptic in general. The eccentricity e_P which varies from 0 to 1 is a measure of the stretching of the polarization ellipse and the two limiting values correspond to a circular and linear polarization, respectively. The angle α_p shows the amount of the ellipse axis rotation with respect to the x direction.

As indicated in Fig. 5 the reflected light is strongly elliptic in a wide range of magnetic fields around the transition point $\varepsilon_B = \Delta_0$ and the eccentricity reaches values even equal to 1, corresponding to linear polarization. In addition, in the region of almost linear polarization, the rotation takes place which becomes more profound for higher frequencies. Far away from the transition region $\varepsilon_B \sim \Delta_0$ the polarization becomes almost circular and almost untwisted since the conductivity tensor becomes isotropic and the time reversal is not broken.

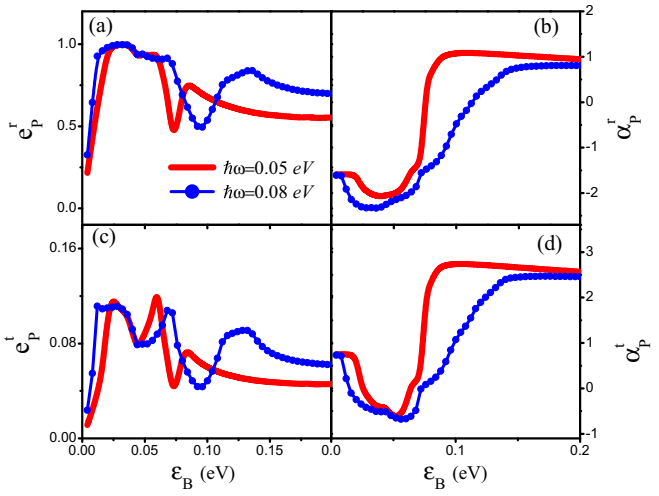

FIG. 5. (Color online) Eccentricity (a),(c) and phase shift (b),(d) of the reflected electromagnetic wave as a function of the magnetic field potential ε_B. The legends in (b)–(d) are the same as in (a).

Similar to the reflected wave, the transmitted part becomes elliptic around $\varepsilon_B \sim \Delta_0$ but its eccentricity shows few peaks which depend on the frequency incident wave. Nevertheless, the ellipticity of the transmitted light is limited and e^t_P reaches values of the order of ∼0.1. The ellipse rotation angles $\alpha^{r,t}_P$ for the reflected and transmitted electromagnetic waves behave almost similarly with constant values at very small and large magnetic fields as seen in Figs. 5(b) and 5(d). Nevertheless, around the transition point $\varepsilon_B \sim \Delta_0$ the ellipses are strongly rotated with a wide range of angles. All these features and the dependence on the frequency can be seen in Fig. 5 where the eccentricity and the rotation angle are plotted as a function of the magnetic energy ε_B.

Up to now we only discussed the optical activity of the thin film with respect to its effect on the polarization of the transmitted and reflected lights. Using Eq. (17) the intensity of absorbed light of the thin film can be obtained and the results are shown in Fig. 6. The ultrathin film of TI is almost transparent and does not absorb the electromagnetic

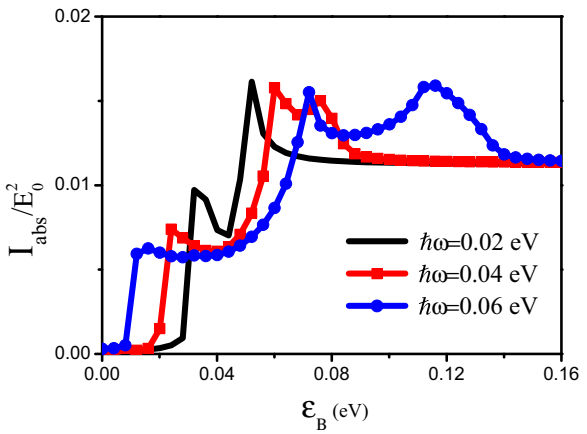

FIG. 6. (Color online) The relative intensity of absorbed light with respect to the incident electromagnetic wave as a function of magnetic field strength for different frequencies ω.

waves with frequencies less than the band gap. Nevertheless by increasing the magnetic field which leads to the phase transition and entrance to the gapless phase an absorption up to a few percent is possible. Moreover, deep inside the gapless phase for very large magnetic fields ($\varepsilon_B \gg \Delta_0$) the absorption becomes independent of the incident light frequency. We also note that $I_{\rm abs}$ reveals a two peak structure which originates from the similar behavior of σ_{yy} as shown in Figs. 4(b) and 4(d).

We conclude our discussion by commenting on the effect of the finite Fermi energy on the results we have presented so far. In fact, the main difference in the presence of a finite doping ($E_{\rm F} \neq 0$) comes from the changes of the lower-lying energy bands in the vicinity of the Fermi level and subsequent variation in the optical transitions from those bands. As far as $E_{\rm F}$ is very smaller to one of the other energy scales Δ_0 and ε_B, the lower energy bands, the selection rules, and the transition matrix elements $\mathcal{J}_{\alpha\beta}$ will not be influenced. Even in the case of the comparable Fermi energy with Δ_0 or ε_B one only expects some shifts in the place of transition peaks in the conductivities versus the frequency of electromagnetic waves. Therefore the qualitative behavior and in particular the anisotropy in the conductivities as well as the presence of peaks and cusps in the frequency dependence remain almost similar to the undoped case. On the other hand, when $E_{\rm F}$ becomes large in comparison with the hybridization energy, then the Fermi level becomes closer or lies within the higher bands and therefore the selection rules and the behavior of conductivities can be different from the undoped case. Particulary, for highly doped thin film in which the Fermi energy is much larger than the hybridization and magnetic cyclotron energies, we expect the disappearance of the anisotropy in the conductivities. Therefore, to observe the effects presented in this paper, it is crucial to have the Fermi energy not being much larger than both of the energy scales Δ_0 and ε_B, a regime which is reliable in the current experimental situations.

IV. CONCLUSIONS

In conclusion, we have investigated the optical responses of an ultrathin topological insulator film in the presence of an in-plane magnetic field B. In the absence of overlap Δ between the surface states of two sides of ultrathin film, such magnetic field can be simply gauged out and its presence will have no physical implications. However, the interplay of the overlap and in-plane magnetic field leads to the physical effect of time-reversal symmetry breaking. Then, the magnetic field results in the strong anisotropy of the optical conductivity, especially when the magnetic energy scale and the overlap are of the same order. At this vicinity, by increasing the magnetic field, the gap of the system closes and a quantum phase transition takes place which also affects the behavior of the optical responses. For instance, in the gapped phase the imaginary part of conductivities dominate while in gapless phase, the dissipative real parts of σ_{xx} and σ_{yy} is much larger.

Our numerical results lead to the strong optical activity of the thin-film TI controllable by the magnetic field strength and the thickness of the film. Assuming a normally incident circularly polarized light, the reflected and transmitted electromagnetic waves are elliptic, in general. In particular, the reflected light can reach high ellipticity and even linear

polarization at the vicinity of the phase transition $\varepsilon_B \sim \Delta_0$. Therefore, the thin film can act as a polaroid for the reflected light. We should mention that since we are dealing with normally incident electromagnetic waves such result must not be mixed with a well-known effect described as Brewster's law. Finally, it is shown that the thin film absorbs the light in the presence of the in-plane magnetic field which can reach up to a few percentage points of the incident intensity.

[1] L. D. Barron, Nature (London) **238**, 17 (1972).
[2] L. D. Barron, Mol. Phys. **43**, 1395 (1981).
[3] P. S. Pershan, J. Appl. Phys. **38**, 1482 (1967).
[4] J. Zak, E. R. Moog, C. Liu, and S. D. Bader, J. Magn. Magn. Mater. **89**, 107 (1990).
[5] A. H. Castro Neto, F. Guinea, N. M. R. Peres, K. S. Novoselov, and A. K. Geim, Rev. Mod. Phys. **81**, 109 (2009).
[6] M. Chhowalla, H. S. Shin, G. Eda, L.-J. Li, K. P. Loh, and H. Zhang, Nat. Chem. **5**, 263 (2013).
[7] M. Z. Hasan and C. L. Kane, Rev. Mod. Phys. **82**, 3045 (2010).
[8] X.-L. Qi and S.-C. Zhang, Rev. Mod. Phys. **83**, 1057 (2011).
[9] L. Fu, C. L. Kane, and E. J. Mele, Phys. Rev. Lett. **98**, 106803 (2007); L. Fu and C. L. Kane, Phys. Rev. B **76**, 045302 (2007).
[10] X.-L. Qi, T. L. Hughes, and S.-C. Zhang, Phys. Rev. B **78**, 195424 (2008); Y. Ando, J. Phys. Soc. Jpn. **82**, 102001 (2013).
[11] Shun-Qing Shen, *Topological Insulator: Dirac Equation in Condesed Matters* (Springer, Heidelberg, 2012).
[12] A. B. Sushkov, G. S. Jenkins, D. C. Schmadel, N. P. Butch, J. Paglione, and H. D. Drew, Phys. Rev. B **82**, 125110 (2010).
[13] G. S. Jenkins, A. B. Sushkov, D. C. Schmadel, N. P. Butch, P. Syers, J. Paglione, and H. D. Drew, Phys. Rev. B **82**, 125120 (2010).
[14] R. Valdés Aguilar, A. V. Stier, W. Liu, L. S. Bilbro, D. K. George, N. Bansal, L. Wu, J. Cerne, A. G. Markelz, S. Oh, and N. P. Armitage, Phys. Rev. Lett. **108**, 087403 (2012).
[15] W.-K. Tse and A. H. MacDonald, Phys. Rev. Lett. **105**, 057401 (2010); Phys. Rev. B **82**, 161104(R) (2010).
[16] W.-K. Tse and A. H. MacDonald, Phys. Rev. B **84**, 205327 (2011).
[17] M. Z. Hasan, Physics **3**, 62 (2010).
[18] X. Xiao and W. Wen, Phys. Rev. B **88**, 045442 (2013); Z. Li and J. P. Carbotte, *ibid.* **87**, 155416 (2013); M. Lasia and L. Brey, *ibid.* **90**, 075417 (2014); X. Wang, J. Lian, Y. Huang, Z. Sun, J. Liu, F. Zhang, S. Gao, X. Yu, P. Li, and M. Zhao, J. Appl. Phys. **52**, 103001 (2013).
[19] H. Rostami and R. Asgari, Phys. Rev. B **89**, 115413 (2014).
[20] N. M. R. Peres and J. E. Santos, J. Phys.: Condens. Matter **25**, 305801 (2013).
[21] K. W. Post, B. C. Chapler, L. He, X. Kou, K. L. Wang, and D. N. Basov, Phys. Rev. B **88**, 075121 (2013); P. Di Pietro, F. M. Vitucci, D. Nicoletti, L. Baldassarre, P. Calvani, R. Cava, Y. S. Hor, U. Schade, and S. Lupi, *ibid.* **86**, 045439 (2012); A. D. LaForge, A. Frenzel, B. C. Pursley, T. Lin, X. Liu, J. Shi, and D. N. Basov, *ibid.* **81**, 125120 (2010).
[22] J. Linder, T. Yokoyama, and A. Sudbo, Phys. Rev. B **80**, 205401 (2009).
[23] C.-X. Liu, H. J. Zhang, B. Yan, X.-L. Qi, T. Frauenheim, X. Dai, Z. Fang, and S.-C. Zhang, Phys. Rev. B **81**, 041307(R) (2010).
[24] H.-Z. Lu, W.-Y. Shan, W. Yao, Q. Niu, and S.-Q. Shen, Phys. Rev. B **81**, 115407 (2010).
[25] Y. Zhang, K. He, C.-Z. Chang, C.-L. Song, L.-LiWang, X. Chen, J.-F. Jia, Z. Fang, X. Dai, W.-Y. Shan, S.-Q. Shen, Q. N., X.-L. Qi, S.-C. Zhang, X.-C. Ma, and Q.-K. Xue, Nat. Phys. **6**, 584 (2010).
[26] W.-Y. Shan, H.-Z. Lu, and S.-Q. Shen, New J. Phys. **12**, 043048 (2010).
[27] H. Li, L. Sheng, D. N. Sheng, and D. Y. Xing, Phys. Rev. B **82**, 165104 (2010).
[28] P. Ghaemi, R. S. K. Mong, and J. E. Moore, Phys. Rev. Lett. **105**, 166603 (2010).
[29] As mentioned in Ref. [37], Zeeman coupling will be as important as gauge field for a thickness above $d = 0.2$ nm; since our samples are thicker than 2 nm we have neglected this term.
[30] A. A. Zyuzin, M. D. Hook, and A. A. Burkov, Phys. Rev. B **83**, 245428 (2011).
[31] N. A. Sinitsyn, J. E. Hill, H. Min, J. Sinova, and A. H. MacDonald, Phys. Rev. Lett. **97**, 106804 (2006).
[32] A. A. Burkov and L. Balents, Phys. Rev. Lett. **107**, 127205 (2011).
[33] M. Tahir, K. Sabeeh, and U. Schwingenschlögl, Sci. Rep. **3**, 1261 (2013).
[34] M. Tahir, A. Manchon, and U. Schwingenschlögl, J. Appl. Phys. **116**, 093708 (2014).
[35] A. A. Zyuzin and A. A. Burkov, Phys. Rev. B **83**, 195413 (2011).
[36] W. E. Liu, H. Liu, and D. Culcer, Phys. Rev. B **89**, 195417 (2014).
[37] S. S. Pershoguba and V. M. Yakovenko, Phys. Rev. B **86**, 165404 (2012).
[38] J. D. Jackson, *Classical Electrodynamics* (Wiley, New York, 1999).